Tampere University

Benjamin Kavanagh

Crystallisation of amorphous TiO$_2$ during vacuum annealing studied by X-ray absorption spectroscopy

ABSTRACT

Benjamin Kavanagh: Crystallisation of amorphous TiO_2 during vacuum annealing studied by X-ray absorption spectroscopy
Bachelor of Science Thesis
Tampere University
April 2021

X-ray Absorption Spectroscopy (XAS) is an analysis method providing elemental specificity and details of the bonding structure in solid state materials. The performance of TiO_2 as a photocatalyst within a photoelectrochemical cell is strongly dependent on its crystal structure. In this work XAS have been used in the analysis of the crystallisation of amorphous TiO_2 under vacuum annealing. Firstly the application of TiO_2 in photoelectrochemical cells as a photocatalyst material has been presented, followed by an overview of the crystalline phases of TiO_2 and their properties. Then the principles of XAS and the experimental set up required to carry out XAS measurements has been discussed. Next is the details of the experimental methods used in this study, including a description of the sample preparation of ALD grown amorphous TiO_2. The XAS measurements conducted and the development of a method of data processing to remove overlapping spectral features. Finally the results of the analysis are presented.

The analysis of the XAS data measured revealed that samples at all 3 ALD growth temperatures crystallised during the annealing process. Using O K-edge reference spectra for rutile and anatase phases led to the identification of the crystallised samples deposited at 100 °C and 150 °C as anatase crystal structure. Furthermore, the temperature at which crystallisation of the amorphous TiO_2 occurs has been identified, revealing a trend that an increase in ALD growth temperature results in a decrease in the temperature required for crystallisation to occur.

Keywords: X-ray Absorption Spectrocopy, photoelectrochemical cell, titanium dioxide, crystallisation

The originality of this thesis has been checked using the Turnitin OriginalityCheck service.

CONTENTS

LIST OF SYMBOLS AND ABBREVIATIONS

E_B	Binding energy of electron
E_{cell}	Electrochemical voltage of a cell
G	Gibb's free energy
$\vec{E}$	Light polarization vector
$\vec{k}$	Photon wave vector
n	Number of moles
ALD	Atomic Layer Deposition
EXAFS	Extended X-ray Absorption Fine Structure
FWHM	Full width at half maximum
GIXRD	Grazing Incidence X-ray Diffraction
HER	Hydrogen Evolution Reaction
NEXAFS	Near Edge X-ray Absorption Fine Structure
OER	Oxygen Evolution Reaction
PEC	Photoelectrochemical Cell
UHV	Ultra High Vacuum (referring to pressures below 10^{-9} mbar)
XANES	X-ray Absorption Near Edge Structure
XAS	X-ray Absorption Spectroscopy

1. INTRODUCTION

One of society's most pressing issues is climate change and the effects of human's power consumption. The need for clean energy sources is of upmost priority if the effects of global warming are to be halted and hopefully even reversed. In 2019 coal still accounted for 36% of global electricity production[1]. The energy striking the earth's surface in the form of sunlight at any time is equal to 130 million 500 MW power plants[2]. If we were able to harness this energy efficiently it would support the world's energy requirements. The development of a solar water splitting cell strives to achieve this. Solar energy can be utilised through the photoelectrochemical splitting of water, using a semiconductor photoelectrode. A photoelectrochemical cell (PEC) converts solar energy into a form that is easily stored and used when required. The energy is stored in the form of H_2 bonds which can later be used as a carbon free energy source in the production of electricity. One of the most widely studied materials for applications within a solar water splitting cell is TiO_2. The properties of which depend on the structure and thus affect the performance of the photoelectrochemical cell.

Within this work an X-ray Absorption Spectroscopy (XAS) analysis of the crystallisation of amorphous TiO_2 is conducted. Firstly the application of TiO_2 within a photoelectrochemical cell for water splitting is discussed along with the crystallisation of TiO_2. Then the fundamentals of XAS and the experimental considerations required are introduced, before moving on to the sample preparation and XAS measurements. Part of the data processing procedure involved the development of a novel method of removal of overlapping photolectron features from the XAS spectra. The motivation in doing this was to allow for comparison with reference spectra which do not contain these overlapping features as well as to increase the value of these results for future research.

The XAS analysis in this study has shown that amorphous TiO_2 crystallises through vacuum annealing, and has identified that for Atomic Layer Deposition (ALD) grown TiO_2 at 100 ℃ and 150 ℃ result in an anatase morphology. Also the results have revealed the temperature at which crystallisation occurs. These findings have potential to aid in the development of solar water splitting cells and the optimization of their efficiency.
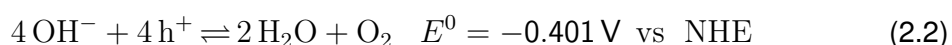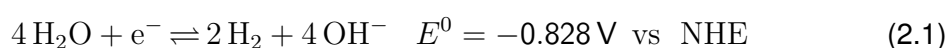
2. APPLICATION OF TiO$_2$ IN PHOTOELECTROCHEMICAL CELLS

The operation of a PEC cell is highly dependent on the materials used, properties of importance to photocatalytic materials include conductivity, stability, crystallinity and cost. Crystalline phases of TiO$_2$ have shown to fulfill these criteria making it a suitable choice as a photocatalyst.

2.1 Water splitting in a photoelectrochemical cell

The main component responsible for the operation of a PEC cell is the semiconductor. Within the semiconductor electron-hole pairs are generated by incident photons. As a result of the electric field within the semiconductor the electron-hole pairs are separated.

The photo generated electrons are transported to the cathode where the reduction of H$_2$O to form H$_2$ takes place. The holes are used at the anode where the oxidation of H$_2$O to form O$_2$ takes place, shown in figure 2.1. Under alkaline conditions the process follows these reactions,

$$4\,H_2O + e^- \rightleftharpoons 2\,H_2 + 4\,OH^- \quad E^0 = -0.828\,V \;\; \text{vs} \;\; \text{NHE} \tag{2.1}$$

$$4\,OH^- + 4\,h^+ \rightleftharpoons 2\,H_2O + O_2 \quad E^0 = -0.401\,V \;\; \text{vs} \;\; \text{NHE} \tag{2.2}$$

The change in Gibb's free energy (ΔG) can be assessed for the reaction, calculated using the formula:

$$\Delta G = -nF\Delta E_{cell}. \tag{2.3}$$

Where n is the amount of substance in moles, F is the Faraday constant and ΔE_{cell} is the electrochemical voltage of the cell. Using the reaction potentials in 2.1 and 2.2 gives $\Delta E_{cell} = -1.229\,V$ and $\Delta G = 118.6\,kJmol^{-1}$ at standard conditions. The positive value of ΔG for the splitting of H$_2$O indicates that the process is non-spontaneous and relies
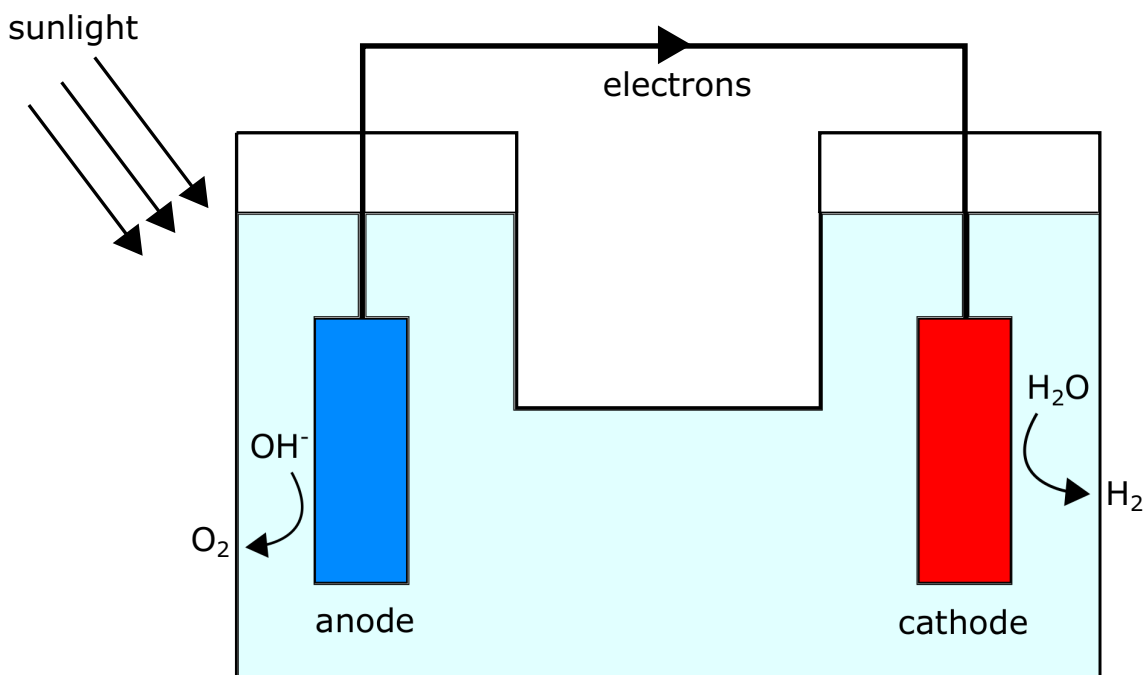
Figure 2.1. *Schematic diagram of a photoelectrochemical cell. The anode is where equation 2.2 takes place and the cathode is where equation 2.1 takes place under alkaline conditions. Figure adapted from [3].*

upon energy input from the PEC cell in order to take place.

However using a semiconductor with a band gap of $1.23\,\text{eV}$, from this theoretically calculated energy, is not sufficient to actually carry out water splitting in practice. Energy losses occur within the semiconductor bulk due to recombination of electron-hole pairs, thermodynamic losses, as well as the overpotentials required at the electrode surface to drive the oxygen evolution reaction (OER) and hydrogen evolution reaction (HER). These overpotentials are influenced by the reaction kinetics, activation energies and are particularly large for the OER as it is the more complex reaction. A realistic range for operating potentials is $1.6\,\text{V}$ to $3.1\,\text{V}$, corresponding to a band gap of $1.6\,\text{eV}$ to $3.1\,\text{eV}$. [2, 4]

2.2 TiO$_2$ as a photocatalyst

The choice of material for the photoanode and cathode are crucial to a PEC cell's performance. The main factors to consider include size and position of band gap, good light absorbance, photo-chemical stability, price and availability. Over the years since Honda and Fujuishima's first success in photoelectrochemically splitting water in 1972 [5], TiO$_2$ has recieved a lot of attention as a photoelectrode material. Like most transition metal oxides TiO$_2$ has a high photochemical stability as well as a band gap which straddles the reduction and oxidation potentials for H$_2$O splitting. However, the large band gap ($3.0\,\text{eV}$ to $3.2\,\text{eV}$ [6]) limits photon absorption within the visible light region.

The large band gap of TiO_2 contributes to the high photochemical stability and is a feature that can be used as an advantage if a thin TiO_2 layer is applied as a protective layer. When combined with another semiconductor with a more favourable band gap and light absorbance range, such as a dual-junction tandem GaInP and GaInAs photoelectrode [7]. Used here TiO_2 has a band alignment which promotes electron transfer between the semiconductor and electrolyte at the cathode surface as well as providing a significant decrease in reflectivity compared with the tandem photoelectrode so increasing the level of light absorbance.

3. CRYSTALLISATION OF TiO$_2$

The chemical properties of TiO$_2$ are dependent on the crystal structure within the material. There are 3 naturally occurring crystalline morphologies for TiO$_2$, being rutile, anatase and brookite. Brookite is rare and has shown to be difficult to synthesise [8]. In this work the focus is on the formation of rutile and anatase from amorphous TiO$_2$. Of these, rutile has the lowest energy and so is the most stable, whilst anatase is metastable [9].

3.1 Crystalline TiO$_2$

The 2 crystalline polymorphs of interest are rutile and anatase, being stable and metastable states of TiO$_2$. The different properties of each are especially important when considering the performance as a photocatalyst, as well as in other applications.

Anatase TiO$_2$ has a tetragonal structure with 12 atoms per unit cell and an experimentally measured band gap of $\sim$3.2 eV. Rutile also has a tetragonal structure with 6 atoms per unit cell and an experimentally measured band gap of $\sim$ 3.0 eV. These structures are presented in Figure 3.1. Both rutile and anatase phases are insoluble in water which is of importance when considering applications in water splitting devices. [8, 10]

There are many parameters contributing to the crystallisation process, each having an effect on the morphology formed. Crystallisation from amorphous to both rutile and anatase phases is possible, as well as the recrystallisation of anatase to rutile, though it is widely accepted that the reverse of this change does not occur [8].

Commonly TiO$_2$ crystallises to anatase more rapidly, a thermodynamical explanation to this could be due to the lower surface free energy of anatase compared to rutile. The surface free energy refers to the increased energy at the surface of a material compared to the bulk and can be viewed as the work required to form a surface.

Rutile is generally formed through exposure to high temperatures, the exact temperature of this is highly dependent on the method of synthesis of TiO$_2$ but is reported to be upwards of 600 °C [8]. The process is not an instantaneous change but is time dependent.
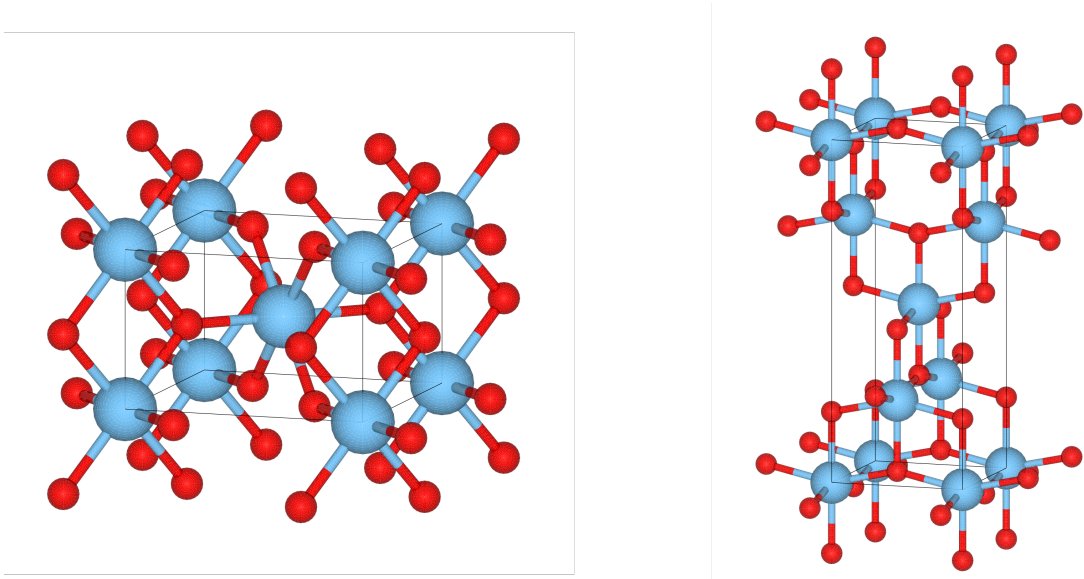
Figure 3.1. *The crystal structure of anatase (left) and rutile (right) TiO$_2$. The large blue atoms spheres represent Ti and small red spheres O. [6]*

3.2 Effect of morphology on photocatalytic performance

Anatase TiO$_2$ is usually considered as having higher photocatalytic performance, there are a number of factors contributing to this. The first of these being the recombination rate in anatase is lower than in rutile. The generation of electron-hole pairs and the recombination are competing processes, where a larger generation to recombination ratio leads to higher photocatalytic activity. Anatase TiO$_2$ is an indirect band gap semiconductor which contributes to the lower recombination rate compared to rutile because direct transition of photo generated electrons from the valence band to conduction band is not possible. [11]

Another contributing factor to photocatalytic performance is the density of adsorbed species. A high density of adsorbed species will enable more charge carriers to be transferred to the adsorbed species. Anatase typically forms a smaller grain size than rutile, which leads to a higher density of adsorbed species and better photocatalytic performance [8, 11]. Studies have also concluded that not only does anatase have a higher surface area but also shows higher photocatalytic activity per unit of surface area [8].

4. X-RAY ABSORPTION SPECTROSCOPY

X-ray Absorption Spectroscopy (XAS) is a measurement technique that provides information enabling the identification of chemical composition and structure. The method is based upon the absorption of X-rays to excite core electrons within the material. When conducting XAS measurements the focus is on the absorption edge. This is a step in absorption intensity at the point where the photon energy is equal to the electron binding energy. The XAS measurement technique is split into 2 common spectroscopy methods.

The first of these being Extended X-ray Absorption Fine Structure (EXAFS) which uses a wide energy range extending hundreds of eV above the absorption edge. This energy range shows low energy oscillations which arise due to the scattering of photoelectrons within the surrounding atoms and interference between the scattered and initial phototelectron waves. Analysis of EXAFS spectra results in detailed information about the bonding of the material including number of neighbouring atoms, bonding distance and type of neighbours. Because of the oscillatory nature of the measured spectra EXFAS lends itself to a Fourier analysis, from which the contributing components can be attributed to a particular bond. However it is usually a complicated analysis procedure because of a large number of variables and requires phase and backscattering amplitudes from reference data [12].

X-ray Absorption Near Edge Structure (XANES) is the other method of XAS and is the one in which this thesis will focus on as it is the spectroscopy method used in analysis of the TiO_2 thin film. XANES measurements are taken over a smaller energy range ($\sim 50\,eV$) around the absorption edge and the focus is on the shape and position of the absorption edge, see Figure 4.1. A fingerprint analysis method is most commonly used, which relies upon the reference spectra from suitable compounds. Analysis of XANES can give element specific information about oxidation states, coordination number and certain bond angles.

4.1 Principles of X-ray Absorption Spectroscopy

The fundamental principles behind XAS rely upon the absorption of X-rays resulting in the excitation of core electrons, usually from the 1s, 2p or 3p orbitals, to unfilled valence states or unbound states. The excitation process leaves core holes within the atom. There
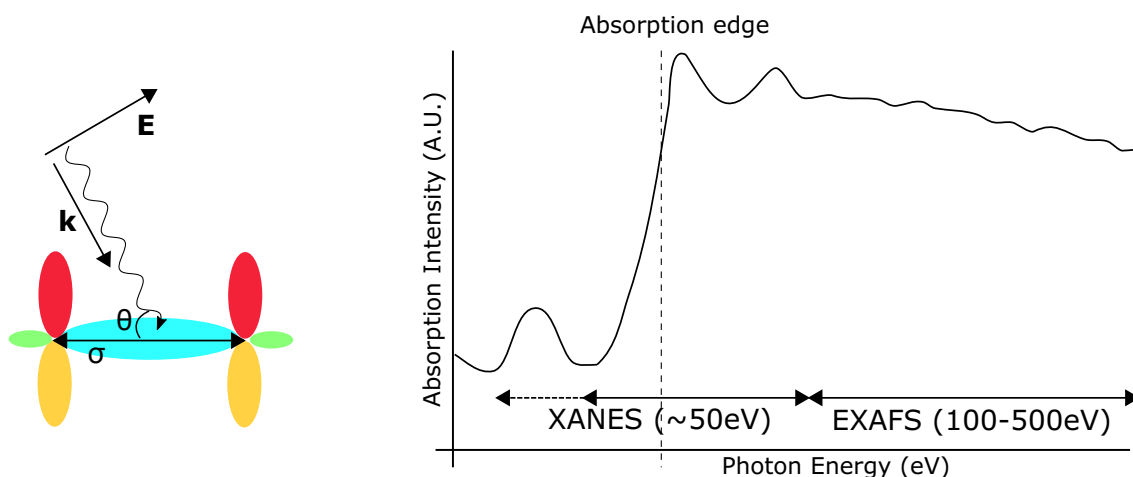
Figure 4.1. *Right presents the energy ranges measured by XANES and EXAFS. On the left is a diagram presenting the orientation of the wave vector ($\vec{k}$), polarization vector ($\vec{E}$) and the electron transition momentum direction. Figure adapted from [13].*

.

are two processes in which relaxation and filling of these core holes can occur, being fluorescence and Auger emission [12]. Both cases involve an electron from a higher state dropping down to fill the core hole and energy is released through fluorescence of a X-ray photon or emission of an Auger electron, shown in figure 4.2.

Like other electron spectroscopy methods, the ability to identify elemental composition directly stems from the involvement of core electrons which are located at characteristic energies for each element. In XAS measurements this translates to the sharp edge located at the binding energy (E_B) of the core electrons. This is due to absorption only taking place when $hv \geq E_B$, where h is Planck's constant and v is the photon's frequency [14]. Dipole selection rules apply to electron transitions between energy states. The conservation of angular momentum requires that the angular momentum quantum number must follow $\Delta l = \pm 1$ [15]. This results in a measurement highly sensitive to the number of valence electrons and local bonding environment of the material.

In XANES the focus is on the shape and position of the absorption edge and the surrounding features. The position of the edge is dependent on the oxidation state and through comparison with reference spectra the local bonding environment can be identified from the shape of the spectral features. The near edge features are as a result of resonant scattering of photoelectrons emitted by the absorbing atom by the surrounding atoms in the immediate vicinity [14]. The features in the absorption intensity can be attributed to a specific electron transition or scattering event [10].

In high ordered structures with a difference in orientation of σ and π bonds, for example some thin films and monolayers, the angle dependence of X-ray absorption can be utilised to determine the orientation of the sample. The angle dependence is proportional to $\sin^2 \theta$ where θ is the angle between the dipole transition momentum of the absorbing
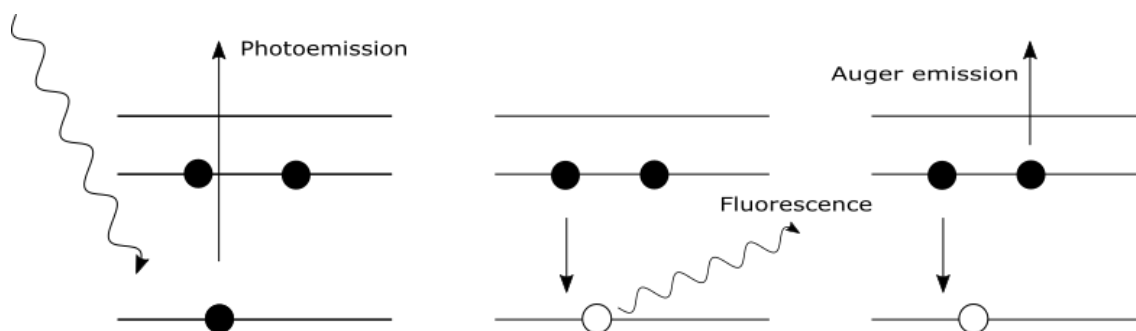
Figure 4.2. *Absorption of an incident X-ray leading to photoemission. Centre shows a core hole being filled through fluorescence. Right shows a core hole being filled through Auger emission.*

electron and the wave vector ($\vec{k}$) of the incident photon, see Figure 4.1. This leads to a maximum probability of absorption occurring when $\vec{k}$ is perpendicular to the dipole transition momentum (or when the polarization vector of the incident radiation ($\vec{E}$) is parallel to the dipole transition momentum) and a minimum is observed when $\vec{k}$ is parallel to the dipole transition momentum[13]. Therefore, through changing the angle θ the contribution of the transitions to π and σ orbitals can be controlled.

4.2 Acquisition of X-ray Absorption Spectra

There are multiple different methods used to conduct XAS measurements. These include total electron yield, Auger electron yield, fluorescence and transmission. Each requires a different experimental set up and the method of choice depends on the samples being measured.

Total electron yield is one of the most commonly used and is performed with the use of a picoammeter connected to the sample to measure the current drain from the sample. Auger electron yield uses an energy analyser to collect and measure the energy of emitted Auger electrons, though this poses the problem that all emitted photoelectrons will also be collected which can lead to overlapping features on the measured spectra. Both total electron yield and Auger electron yield have the limitation that the measured spectra are effected by sample charging and so this should be considered when studying samples with low conductivity.

Fluorescence involves measuring the energy of the fluorescent photons emitted but has the limitation on applicability for elements with a small atomic number that have a low probability of fluorescence[13]. Transmission measurements have the limitation of only being applicable to thin samples where the incident and transmission intensities of the X-ray is measured and the absorption coefficient is proportional to the logarithm of these. Additionally, transmission measurements are best suited for applications when studying higher energy edges, since absorption in the soft x-ray range ($<5\,\mathrm{keV}$) is very high and

so imposes a very small limit on the sample thickness.

4.3   Synchrotron light source

Conducting an XAS measurement involves scanning of the incident X-ray energy across the appropriate energy range for the absorption edge of interest. Due to the requirements of a tunable energy source with high photon flux and high spectral resolution it is not possible to conduct XAS measurements in a standard laboratory. Normal laboratory X-ray sources are limited to specific excitation energies dependent on the anode material. These are dependent on the anode material but often these are Al k_{α} and Mg k_{α} at 1486.6 eV and 1253.6 eV respectively. Hence the use of synchrotron radiation is the most appropriate X-ray source for conducting XAS measurements.

Synchrotron radiation refers to a continuous band of electromagnetic radiation covering infrared, visible light, ultraviolet and X-rays. It is produced with the use of high energy electrons travelling near the speed of light. When these electrons are deflected by a magnetic field photons are emitted in a thin beam tangential to the electron's direction of travel and with an intensity proportional to the curvature of the electrons [16].

In order to produce synchrotron radiation large specialised facilities are required. These consist of a large storage ring, normally 100 m to 1000 m in circumference, consisting of an evacuated pipe containing electrons at relativistic velocities [17]. Electrons are injected into the storage ring by electron guns to maintain a constant current. Within the storage rings are multiple magnets to guide the electrons round the ring, and series of insertion devices. The insertion devices are constructed from a series of alternating magnets which cause the electron beam to oscillate and thus emit a photon beam. There are two types of insertion devices: wrigglers which cause multiple changes of direction of the electrons and generate a short wavelength of high intensity light; undulators which cause a periodic change of direction of the electrons and generate ultra-brilliant radiation concentrated to specific energy values within an energy range as a result of the interference patterns produced.

The synchrotron radiation produced is passed through a series of slits, optical devices and monochromators (referred to as a beamline) designed to focus and monochromatise the radiation on the sample at the experimental endstation. In this work the beamline used for measurements uses an undulator to produce the X-ray radiation [18].

5. EXPERIMENTAL PROCEDURE

This chapter provides a description of the experimental procedure of this study, including sample preparation and collection of the XAS measurements. The developed method for removal of overlapping spectral features within the collected XAS spectra is then described.

5.1   Sample preparation

A 30 nm layer of TiO_2 was deposited using ALD in a Picosun Sunale R-200 advanced reactor. The deposition was made using Tetrakis(dimethylamido)titanium(IV) (TDMAT) precursor and deionized water as the reactant. The film was applied onto $Si-100$ wafer at deposition temperatures of 100 ℃, 150 ℃ and 200 ℃. The resulting TiO_2 layer is known to be amorphous.

After ALD depositions of TiO_2, the samples were subject to 1 week of atmospheric exposure during transportation to the synchrotron facility. The samples were then annealed to 200 ℃, 250 ℃, 300 ℃, 350 ℃, 400 ℃, 450 ℃ and 500 ℃ in-situ under vacuum conditions. The annealing was conducted cumulatively, using the same sample for each temperature. Each stage of the annealing consisted of 30 minutes annealing time including the heating of the sample to target temperature. This was conducted by heating at a constant power, required for the target temperature, resulting in a quick ramp in temperature to a value close to the target temperature.

5.2   XAS measurements

XAS measurements were conducted at the FinEstBeAMS beamline at MAX IV laboratory in Sweden. The beamline has 2 branches, supplying the solid state end station used in this work and a gas phase end station. Further details of the beamline can be found elsewhere[18]. Spectra were collected in between each stage of annealing. All measurements were taken using Auger electron yield with the use of a hemispherical electron energy analyzer to collect emitted Auger electrons. The energy range measured was 510.3 eV to 515.7 eV, corresponding to the energy of an intense Auger emission. The incident photon energy was then scanned over the O K-edge.
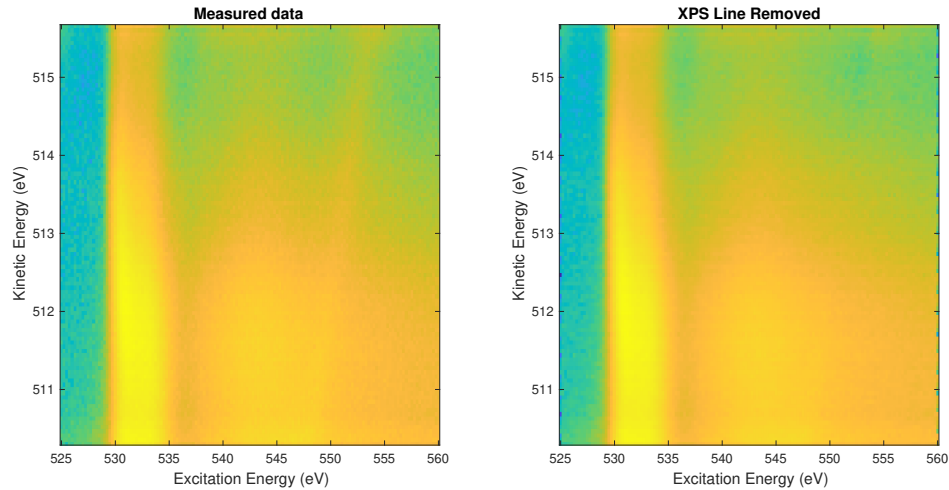
Figure 5.1. *XAS data of ALD grown TiO$_2$ at* 100 ℃ *after annealing at* 100 ℃ *before and after removal of the overlapping peak. The photoelectron peak is the diagonal line of intensity seen in the measured data.*

All measurements were conducted at pressure in the 10^{-10} mbar range and at room temperature. The photon flux was recorded during the measurements, allowing the intensity to be normalized before processing the data.

5.3 Removal of overlapping spectral features

The measured XAS spectra contain overlapping photoelectron features. These arise due to photoemission from energy states at a binding energy which results in emission of a photoelectron of kinetic energy within the measured range. The binding energy of the photoelectron is given by

$$KE = E_{photon} - E_{BE} - \Phi. \tag{5.1}$$

Where KE is the kinetic energy of the emitted photoelectron, E_{photon} is the energy of the excitation energy source, E_{BE} is the binding energy from where the photoelectron originates and Φ is the spectrometer work function [19]. Using this gives $E_{BE} = 37.8$ eV, corresponding to the Ti 3p photoelectron peak.

The overlapping photoelectron peak is visible as the diagonal line of high intensity in the measured data in Figure 5.1. This feature is present in all of the measured spectra so a comparison between each of them would be possible, however comparison to reference spectra measured under different conditions would not be possible. As the lack of an identical overlapping photoelectron feature could cause difficulty in interpretation of the results and/or misinterpretation leading to incorrect conclusions. Also the fact that the overlapping feature corresponds to the Ti 3p state means that the shape of the photoelectron

feature may change during the annealing process causing further difficulty in interpreting the spectra. So in order to draw conclusions from this data a method of removing the overlapping spectral features has been developed.

The method for removing these overlapping photoelectron features is described here. First the 2 dimensional spectra were skewed to vertically align the photoelectron peak, this was done to make the data processing easier as the photoelectron peak was confined within a range of columns. A 3rd order polynomial was then fitted to the spectra using 3-5 data points from either side of the photoelectron peak. Linear and different order polynomials were tried when developing this method, but the 3rd order polynomial was shown to provide the most reliable prediction of the background spectra. A possible reason for this could be down to the number of parameters that allows the fitting to align to the gradient of the spectra at either side of the photoelectron feature, but doesn't allow for overly complex fitting shapes as was experienced with higher order polynomials. The photoelectron peak shape was then calculated by subtracting the fitting from the appropriate portion of the measured spectra. Finally, this photoelectron peak shape was subtracted from the skewed spectra before reversing the skew.

Before analysis the 2 dimensional spectra were summed to give Auger electron yield intensity as a function of photon energy. These spectra were normalized to the post edge step heights, as is common practice.

6. RESULTS AND ANALYSIS

This chapter presents the measured data described in Chapter 5. A fingerprint analysis of the XANES spectra was conducted with the aid of reference spectra that were prepared in the same laboratory and measured at the same synchrotron facility.

6.1 Crystal structure after vacuum annealing

A comparison of the Oxygen K-edge spectra at different annealing temperatures on each of the 3 amorphous TiO_2 films studied is presented in Figure 6.1 along with anatase and rutile reference spectra. All samples studied exhibit the same spectral features, consisting of 2 main peaks centred at around $\sim 530.8\,\text{eV}$ and $533\,\text{eV}$, as well as an additional feature at higher energies. This is consistent with previous XAS studies on TiO_2 [10, 12].

All 3 deposition temperatures show a similar trend at higher annealing temperatures; the 2 main peaks have a larger energy separation as well as a sharpening of the spectral features. These changes are indications that crystallisation has occurred [10]. Amorphous TiO_2 produces broadened features as apposed to rutile and anatase, this is due to small variations in bond lengths and angles between atoms.

The features of the O K-edge can be explained using the molecular orbital model of TiO_2. The conduction band consists of antibonding Ti $3d$, $4s$ and $4p$ and O $2p$ orbitals. The crystal field formed by the surrounding O atoms causes the splitting of the Ti $3d$ orbital into sub bands e_g and t_{2g}. The transition responsible for the main peak in the O K-edge spectra is from the O $1s$ core level to the e_g and t_{2g} sub bands, corresponding to the higher energy component and lower energy component of the main peak respectively. The e_g sub band is most sensitive of these to the surrounding environment because its' orientation points towards the O $2p$ orbitals. The other features at higher energies arise from transitions into the other antibonding O 2p and Ti 3s and 3p bands. [10]

Rutile and anatase morphologies exhibit a similar peak separation between the 2 main peaks and so it is not possible to distinguish the crystal structure from these features. However there are noticeable differences in the shape of the feature at higher excitation energy. Reference spectra in Figures 6.1, 6.2 show a characteristic flat top to the higher energy feature of rutile, as well as a less pronounced shoulder on the lower energy side.
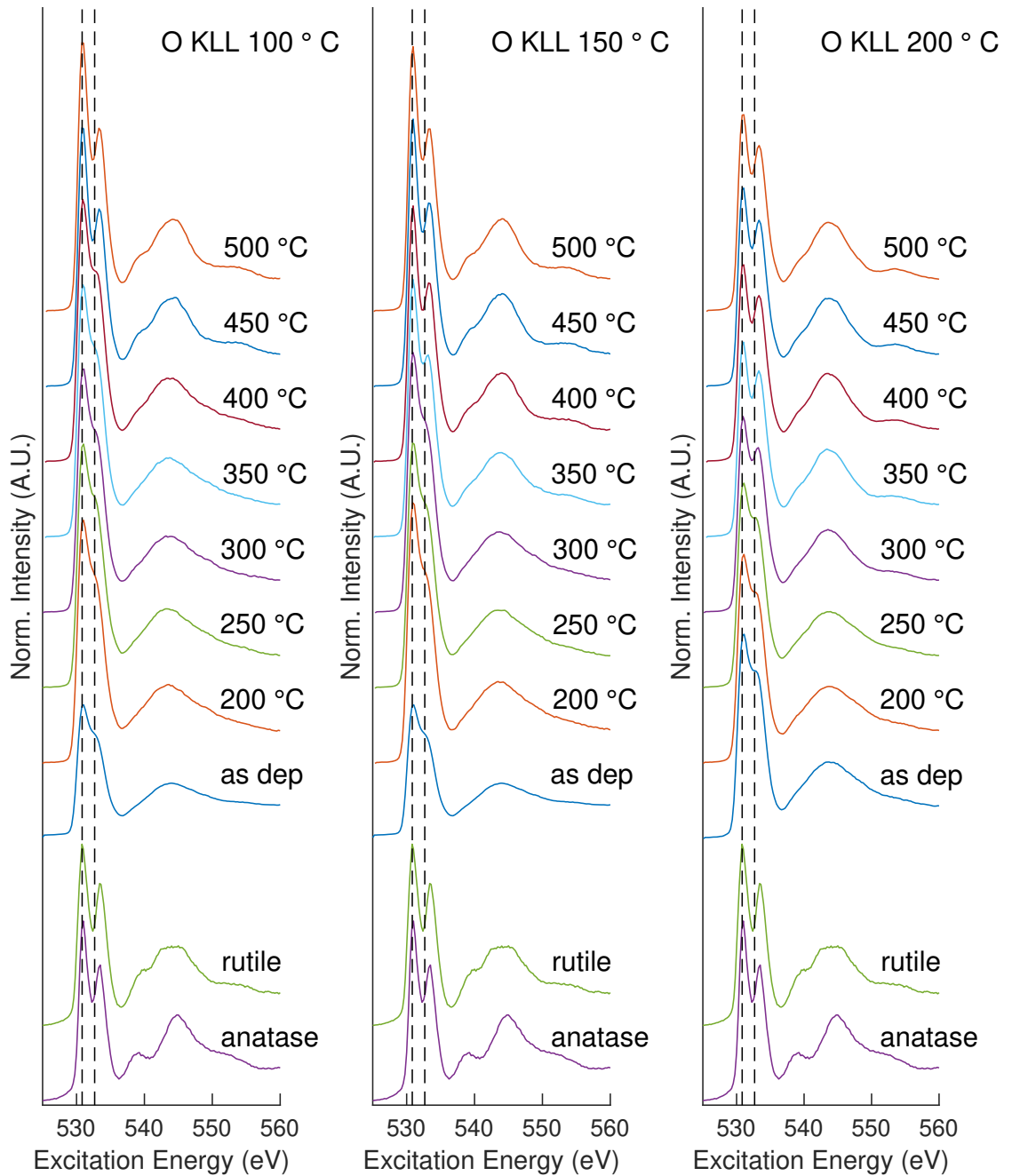
Figure 6.1. *Measured XAS spectra of O KLL edge for each sample. Peak positions of the as deposited spectra are marked by the dashed lines.*

Using these differences allows a possible distinction between rutile and anatase to be made.

A closer comparison of the peak shapes of the higher energy feature is presented in Figure 6.2. From this it is clear that the ALD depositions at 100 °C and 150 °C share a very similar shape, but the 200 °C sample differs from these. The lower energy side of the 200 °C peak shows an almost linear shape whereas the 100 °C and 150 °C have an 'S' shape more similar to the anatase reference data. Using these differences suggests that ALD depositions at 100 °C and 150 °C crystallise to anatase. The morphology of the
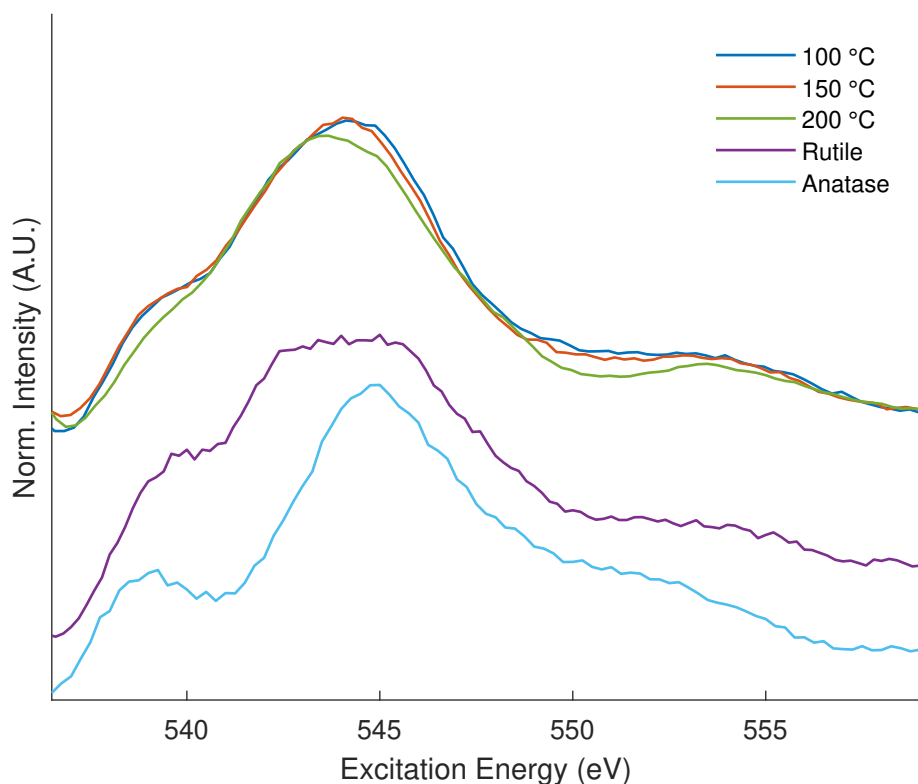
Figure 6.2. *A comparison of the shape of the lower intensity O KLL feature after anneal-ing.* 100 °C *and* 150 °C *samples match closely to anatase reference.*

200 °C is less clear but the difference in peak shape suggests a possible rutile morphology, however these XAS measurements are not sufficient to draw a definite conclusion on the crystalline structure after annealing.

Analysis of these samples using Grazing Incidence X-ray Diffraction (GIXRD) after the annealing process confirmed the morphologies of the 100 °C and 150 °C samples as being anatase. However the structure of the 200 °C sample was also unclear. The measurement data have been attached in Appendix A as it is out of the scope of this thesis.

6.2 Crystallisation temperature during vacuum annealing

The temperature at which crystallisation occurs for each of the samples can be determined by analysis of the peak separation of the main feature of the O K-edge. A peak fitting was made using 2 Gaussian curves, from which the peak separation was calculated using the difference of the component positions. The peak separation as a function of annealing temperature is shown in Figure 6.3. A sharp increase in the peak separation for all of the samples is observed, which as previously mentioned serves as an indicator to the temperature at which crystallisation occurs.

A trend in the temperature required for crystallisation is apparent; an increase in ALD
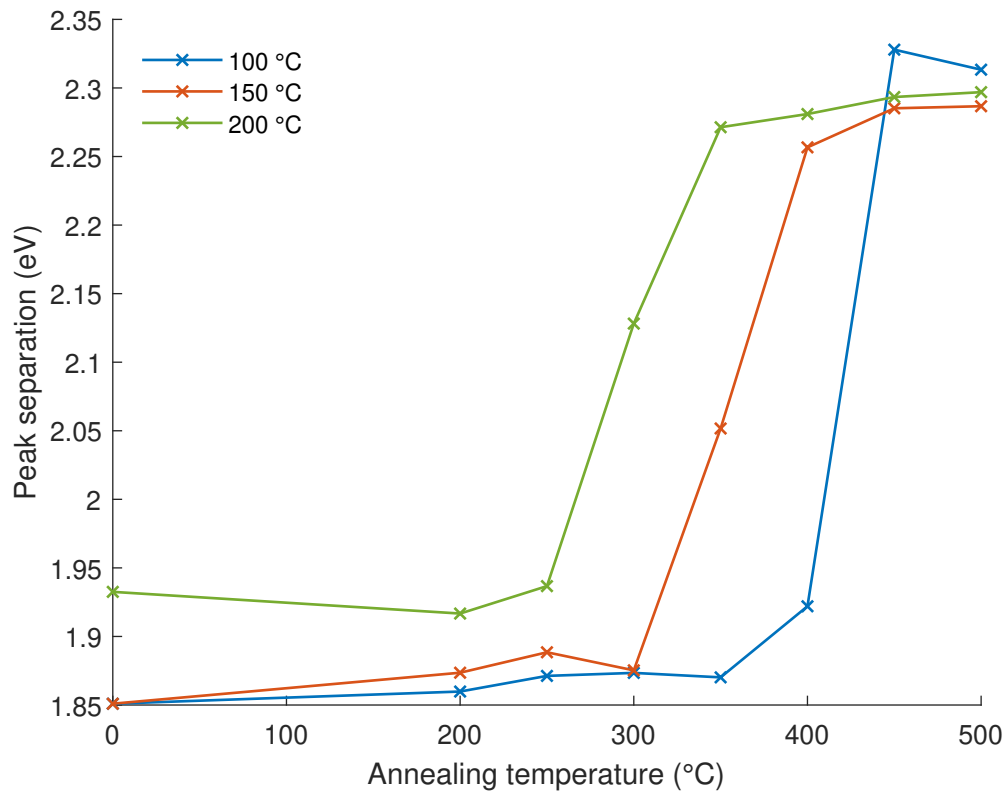
Figure 6.3. *Peak separation of the two components of the main feature from the O K-edge at each annealing temperature.*

deposition temperature leads to a decrease in annealing temperature required for crystallisation. In the 100 °C sample crystallisation occurs with annealing to 450 °C, the 150 °C crystallises at 350–400 °C and the 200 °C crystallises at 300–350 °C.

To confirm the results drawn from the analysis of the peak separation the Full Width at Half Maximum (FWHM) of the two components of the main feature were analysed. The component at lower energy remained constant during annealing, but the component at higher energy showed a sharpening (decrease in FWHM) at the point when crystallisation occurred, this is presented in Figure 6.4. The temperatures at which this was observed are consistent with the temperatures of crystallisation identified through analysis of the peak separation.
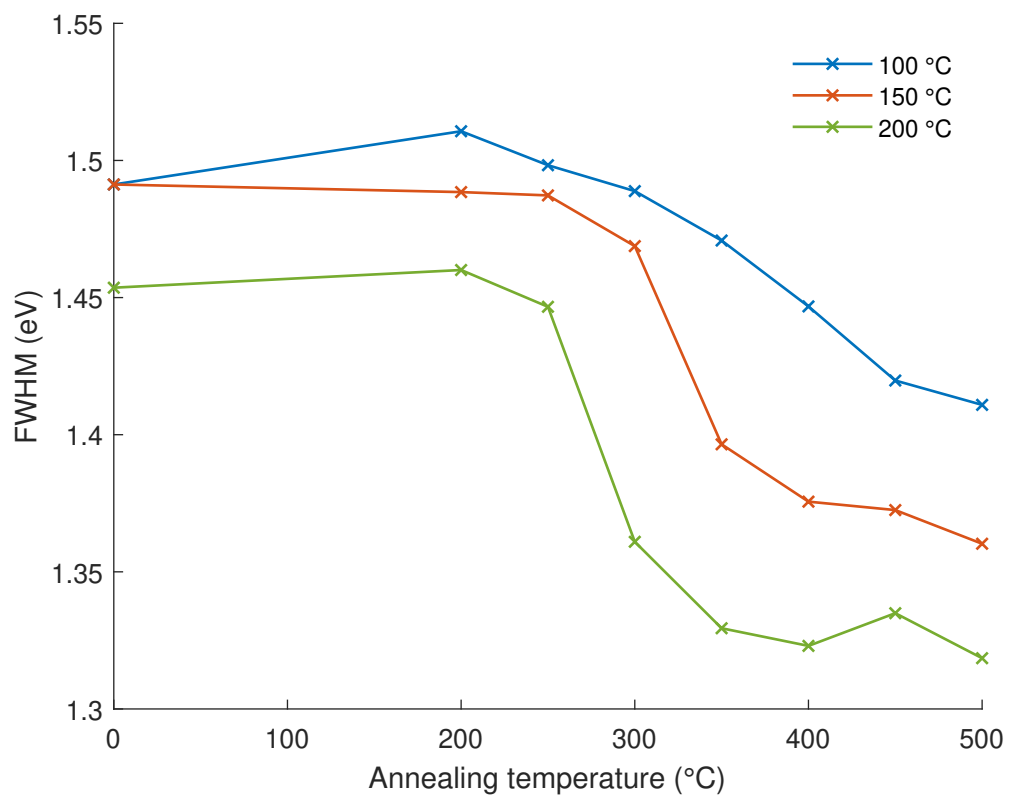
Figure 6.4. *FWHM of the higher energy component of the main feature from the O K-edge at each annealing temperature.*

7. CONCLUSION

In this work the crystallisation of amorphous TiO_2 has been studied through the analysis of XAS data. The theoretical background regarding the crystallisation of TiO_2, one of its applications as a photocatalyst within a solar water splitting cell and the fundamentals behind XAS measurements have been presented. Furthermore a method of processing the XANES data to remove overlapping photoelectron peaks has been developed which enables comparison of the measured data to reference spectra.

The XANES analysis of the crystallisation of amorphous TiO_2 has identified that the ALD thin films grown at 100 ℃ and 150 ℃ have crystallised to anatase crystal structure. This is consistent with literature that amorphous TiO_2 crystallises more readily to anatase at lower temperatures. The results of the thin film grown at 200 ℃ were less conclusive, but obvious differences in the spectral feature shapes have led to speculate that this has crystallised to rutile, though there is insufficient data to be confident in this. It should be noted that GIXRD measurements of these samples have came to the same conclusion as found in this study.

The analysis has also lead to the identification of the temperature of crystallisation of amorphous TiO_2 under vacuum annealing. Through analysis of the peak splitting of the O K-edge and the change in peak width a trend was identified; an increase in ALD growth temperature leads to a decrease in the temperature required for crystallisation to occur. The thin film grown at 100 ℃ crystallised at 450 ℃, compared to the film grown at 200 ℃ that crystallised at 300–350 ℃. Analysis of both peak separation and peak width yielded the same results.

To conclude XAS has been presented as a spectroscopy technique with elemental specificity and the possibility to identify chemical states and bond structure through the involvement of core and valence band electrons. The use of XAS in this thesis has identified the crystal structure of anatase TiO_2, although has left some ambiguity as to the crystal structure of one sample. This leaves potential for a further study into the structure of the vacuum annealed sample ALD grown at 200 ℃. This serves as a reminder that there is rarely one spectroscopy method that is capable of identifying every aspect of a material and that a combination of spectroscopy methods is often required.

REFERENCES

[1] IEA. *Global Energy Review 2020*. 2020. URL: https://www.iea.org/reports/global-energy-review-2020.

[2] Walter, M. G., Warren, E. L., McKone, J. R., Boettcher, S. W., Mi, Q., Santori, E. A. and Lewis, N. S. Solar Water Splitting Cells. *Chemical Reviews* 110.11 (2010). PMID: 21062097, pp. 6446–6473. DOI: 10.1021/cr1002326. eprint: https://doi.org/10.1021/cr1002326. URL: https://doi.org/10.1021/cr1002326.

[3] Ahmad, H., Kamarudin, S., Minggu, L. and Kassim, M. Hydrogen from photo-catalytic water splitting process: A review. *Renewable and Sustainable Energy Reviews* 43 (2015), pp. 599–610. ISSN: 1364-0321. DOI: https://doi.org/10.1016/j.rser.2014.10.101. URL: https://www.sciencedirect.com/science/article/pii/S1364032114009265.

[4] Roel van de Krol, M. G. *Photoelectrochemical Hydrogen Production*. Springer, 2012.

[5] Fujishima, H. *Nature* (1972). DOI: 10.1038/238037a0. URL: https://doi.org/10.1038/238037a0.

[6] Ali, I., Suhail, M., Alothman, Z. A. and Alwarthan, A. Recent advances in syntheses, properties and applications of TiO2 nanostructures. *RSC Adv.* 8 (53 2018), pp. 30125–30147. DOI: 10.1039/C8RA06517A. URL: http://dx.doi.org/10.1039/C8RA06517A.

[7] Cheng, W.-H., Richter, M. H., May, M. M., Ohlmann, J., Lackner, D., Dimroth, F., Hannappel, T., Atwater, H. A. and Lewerenz, H.-J. Monolithic Photoelectrochemical Device for Direct Water Splitting with 19% Efficiency. *ACS Energy Letters* 3.8 (2018), pp. 1795–1800. DOI: 10.1021/acsenergylett.8b00920. eprint: https://doi.org/10.1021/acsenergylett.8b00920. URL: https://doi.org/10.1021/acsenergylett.8b00920.

[8] Dorian A. H. Hanaor, C. C. S. Review of the anatase to rutile phase transformation. *Journal of Materials Science* (Jan. 2011), pp. 855–874. URL: https://doi.org/10.1007/s10853-010-5113-0.

[9] Agirseven, O., Rivella, D. T., Haggerty, J. E. S., Berry, P. O., Diffendaffer, K., Patterson, A., Kreb, J., Mangum, J. S., Gorman, B. P., Perkins, J. D., Chen, B. R., Schelhas, L. T. and Tate, J. Crystallization of TiO2 polymorphs from RF-sputtered, amorphous thin-film precursors. *AIP Advances* 10.2 (2020), p. 025109. DOI: 10.1063/1.5140368. URL: https://doi.org/10.1063/1.5140368.

[10]   Kucheyev, S. O., Buuren, T. van, Baumann, T. F., Satcher, J. H., Willey, T. M., Meu-
        lenberg, R. W., Felter, T. E., Poco, J. F., Gammon, S. A. and Terminello, L. J. Elec-
        tronic structure of titania aerogels from soft x-ray absorption spectroscopy. *Phys.
        Rev. B* 69 (24 June 2004), p. 245102. DOI: `10.1103/PhysRevB.69.245102`. URL:
        `https://link.aps.org/doi/10.1103/PhysRevB.69.245102`.

[11]   Zhang, J., Zhou, P., Liu, J. and Yu, J. New understanding of the difference of pho-
        tocatalytic activity among anatase, rutile and brookite TiO2. *Phys. Chem. Chem.
        Phys.* 16 (38 2014), pp. 20382–20386. DOI: `10.1039/C4CP02201G`. URL: `http:
        //dx.doi.org/10.1039/C4CP02201G`.

[12]   Chen, J. NEXAFS investigations of transition metal oxides, nitrides, carbides, sul-
        fides and other interstitial compounds. *Surface Science Reports* 30 (1997), pp. 1–
        152.

[13]   Vinogradov, N. *Controlling Electronic and Geometrical Structure of Honeycomb-
        Lattice Materials Supported on Metal Substrates*. Uppsala University, 2013, p. 103.

[14]   Niemantsverdriet, W. *Spectroscopy in Catalysis*. Wiley-VCH, 2007. 325 p.

[15]   Soriano, L., Abbate, M., Vogel, J., Fuggle, J., Fernández, A., González-Elipe, A.,
        Sacchi, M. and Sanz, J. Chemical changes induced by sputtering in TiO2 and some
        selected titanates as observed by X-ray absorption spectroscopy. *Surface Science*
        290.3 (1993), pp. 427–435. ISSN: 0039-6028. DOI: `https://doi.org/10.1016/
        0039-6028(93)90725-Y`. URL: `https://www.sciencedirect.com/science/
        article/pii/003960289390725Y`.

[16]   Heide, P. van der. *X-ray Photoelectron Spectroscopy*. John Wiley Sons, 2011. 262
        p.

[17]   Bunker, G. *Introduction to XAFS*. Cambridge University Press, 2010. 270 p.

[18]   Pärna, R., Sankari, R., Kukk, E., Nõmmiste, E., Valden, M., Lastusaari, M., Kooser,
        K., Kokko, K., Hirsimäki, M., Urpelainen, S., Turunen, P., Kivimäki, A., Pankratov,
        V., Reisberg, L., Hennies, F., Tarawneh, H., Nyholm, R. and Huttula, M. FinEst-
        BeaMS – A wide-range Finnish-Estonian Beamline for Materials Science at the
        1.5GeV storage ring at the MAX IV Laboratory. *Nuclear Instruments and Methods
        in Physics Research Section A: Accelerators, Spectrometers, Detectors and Asso-
        ciated Equipment* 859 (2017), pp. 83–89. ISSN: 0168-9002. DOI: `https://doi.
        org/10.1016/j.nima.2017.04.002`. URL: `https://www.sciencedirect.
        com/science/article/pii/S0168900217304230`.

[19]   Moulder, J., Stickle, W., Sobol, P. and Bomben, K. *Handbook of X-ray Photoelectron
        Spectroscopy*. Perkin Elmer Corporation, 1992.

APPENDIX A: GRAZING INCIDENCE X-RAY DIFFRACTION SPECTRA OF TiO$_2$

The measured GIXRD spectra are presented in A.1. Comparison of the measured spectra to reference spectra reveal that before annealing all samples are amorphous. After
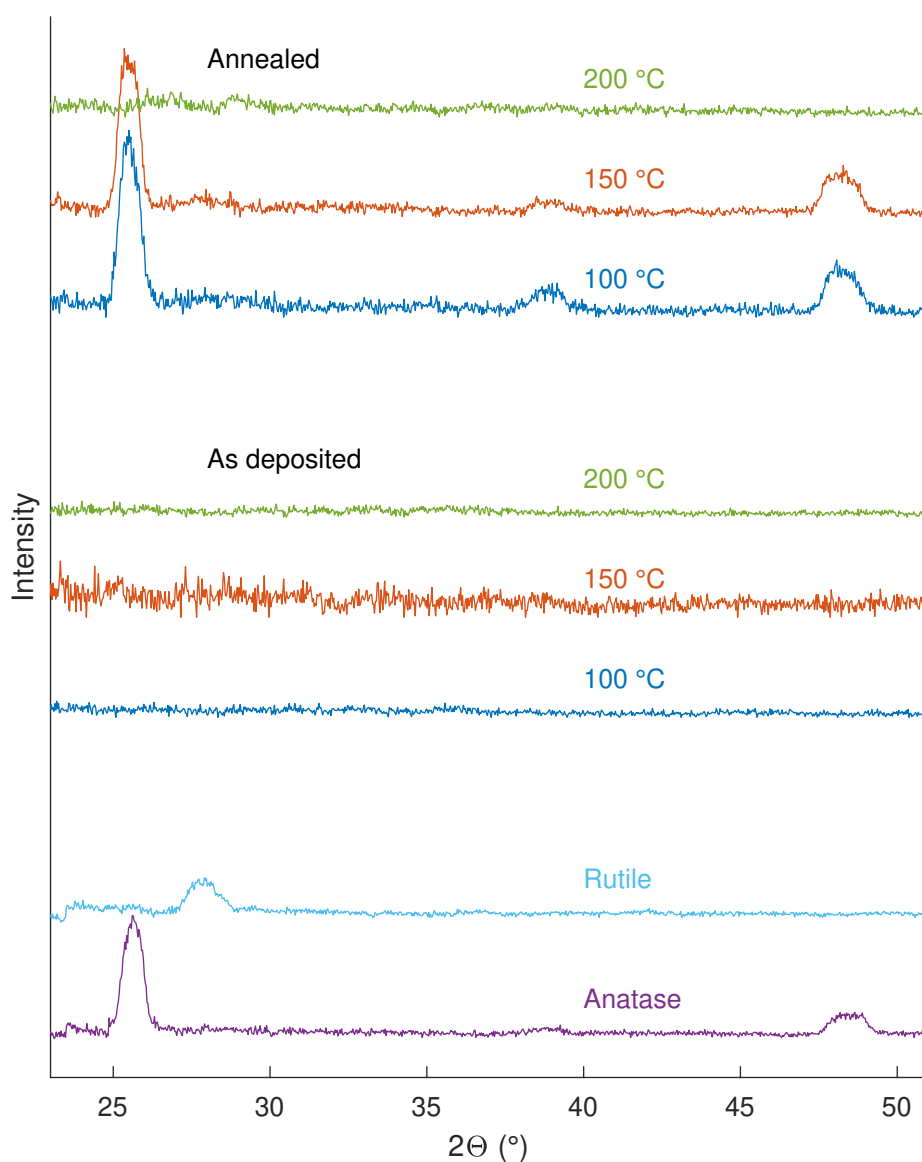

Figure A.1. *Measured GIXRD spectra of the TiO$_2$ samples studied, before and after annealing, alongside reference spectra for Rutile and Anatase phases.*

annealing the TiO_2 grown at 100 ℃ and 150 ℃ are of anatase morphology and the data for 200 ℃ does not reveal the crystal structure. These results are consistent with what was found in the XAS analysis.